

# Ten years of INTEGRAL observations of the hard X-ray emission from SGR 1900+14 (Research Note)

L. Ducci<sup>1,2</sup>, S. Mereghetti<sup>3</sup>, D. Götz<sup>4</sup>, and A. Santangelo<sup>1</sup>

<sup>1</sup> Institut für Astronomie und Astrophysik, Eberhard Karls Universität, Sand 1, 72076 Tübingen, Germany  
e-mail: ducchi@astro.uni-tuebingen.de

<sup>2</sup> ISDC Data Center for Astrophysics, Université de Genève, 16 chemin d'Écogia, 1290 Versoix, Switzerland

<sup>3</sup> INAF – Istituto di Astrofisica Spaziale e Fisica Cosmica, Via E. Bassini 15, 20133 Milano, Italy

<sup>4</sup> AIM (UMR 7158 CEA/DSM-CNRS-Université Paris Diderot) Irfu/Service d'Astrophysique, Saclay, F-91191 Gif-sur-Yvette Cedex, France

Received ...; accepted ...

## ABSTRACT

We exploited the high sensitivity of the INTEGRAL IBIS/ISGRI instrument to study the persistent hard X-ray emission of the soft gamma-ray repeater SGR 1900+14, based on  $\sim 11.6$  Ms of archival data. The 22–150 keV INTEGRAL spectrum can be well fit by a power law with photon index  $1.9 \pm 0.3$  and flux  $F_x = (1.11 \pm 0.17) \times 10^{-11}$  erg cm<sup>-2</sup> s<sup>-1</sup> (20 – 100 keV). A comparison with the 20–100 keV flux measured in 1997 with *BeppoSAX*, and possibly associated with SGR 1900+14, shows a luminosity decrease by a factor of  $\sim 5$ . The slope of the power law above 20 keV is consistent within the uncertainties with that of SGR 1806–20, the other persistent soft gamma-ray repeater for which a hard X-ray emission extending up to 150 keV has been reported.

**Key words.** gamma-rays: observations – pulsars: individual SGR 1900+14 – pulsars: general

## 1. Introduction

Soft Gamma-ray Repeaters (SGRs), together with Anomalous X-ray Pulsars (AXPs), are high energy sources which are thought to be magnetars, i.e. neutron stars whose emission is powered mainly by their strong magnetic field (see Mereghetti et al. 2015 for a recent review).

SGRs show recurrent short bursts (typical duration of the order of  $\approx 0.1$  s) in the X-ray and soft gamma-ray range, with peak luminosities of  $10^{39} - 10^{42}$  erg s<sup>-1</sup> for normal bursts and up to  $\approx 10^{47}$  erg s<sup>-1</sup> for “giant flares”. Bursts are usually emitted during active states that can last from a few days to months. Active states are interrupted by long quiescent (or non-bursting) time intervals with persistent luminosities of  $\approx 10^{33} - 10^{36}$  erg s<sup>-1</sup>.

In this paper we make use of the archival data of the International Gamma-Ray Astrophysics Laboratory (INTEGRAL, Winkler et al. 2003) collected in the period 2003–2013 to study the hard X-ray emission (above 20 keV) from SGR 1900+14.

Since the launch of INTEGRAL, SGR 1900+14 has shown only two periods of bursting activity: November 2002 (Hurley et al. 2002) and March 2006 (Vetere et al. 2006; Golenetskii et al. 2006). Its persistent emission has been extensively studied, especially in the soft X-ray range ( $\leq 10$  keV) with *XMM-Newton* (e.g. Mereghetti et al. 2006), *Chandra* (e.g. Göğüş et al. 2011), *Suzaku* (Nakagawa et al. 2009), and *BeppoSAX* (Tiengo et al. 2007; Esposito et al. 2007). The *XMM-Newton* and *Suzaku* spectra (0.8–10 keV) are well fit either by an absorbed ( $N_H \approx 2.1 \times 10^{22}$  cm<sup>-2</sup>) power law ( $\Gamma \approx 1.9$  for *XMM-Newton*,  $\Gamma \approx 2.8$  for *Suzaku*) plus a blackbody component ( $kT \approx 0.5$  keV) or by two absorbed blackbodies ( $kT_1 \approx 0.5$  keV,  $kT_2 \approx 1.9$  keV; Mereghetti et al. 2006; Nakagawa et al.

2009). Persistent hard X-ray emission from SGR 1900+14 in the 20–100 keV has been discovered by Götz et al. (2006) using observations obtained with INTEGRAL in the period 2003–2004. The hard X-ray emission detected with INTEGRAL was fit by a power law with photon index  $\Gamma \sim 3.1$ , significantly steeper than that of other SGRs and AXPs (Götz et al. 2006). Esposito et al. (2007) reported the detection of hard (20–150 keV) X-ray emission from a region around SGR 1900+14 with the non-imaging spectrometer PDS (Phoswich Detection System, Frontera et al. 1997) on board the *BeppoSAX* satellite. They modeled the observed X-ray emission with a power law with slope  $\Gamma \approx 1.6$ . Three transient X-ray sources were located within the PDS field of view, but none of them was in a bright state during the observation of SGR 1900+14. Therefore, the X-ray emission detected by *BeppoSAX* was likely produced by SGR 1900+14, although the contamination from other unknown transient sources within the PDS field of view cannot be ruled out (Esposito et al. 2007).

The hard X-ray emission of SGR 1900+14 has been studied so far with a limited set of data. In this work, we exploit  $\sim 10$  years of archival INTEGRAL data to further investigate the properties of its emission above 20 keV, and put them in the broader context of the class of magnetars. In Sect. 2 we present the INTEGRAL observations on which our work is based, the data analysis procedure, and the results, that are then discussed in Sect. 3.

## 2. Data analysis and results

We used data obtained with the ISGRI (INTEGRAL Soft Gamma-Ray Imager, Lebrun et al. 2003) detector of the coded-mask telescope IBIS (Imager on board INTEGRAL Satellite,

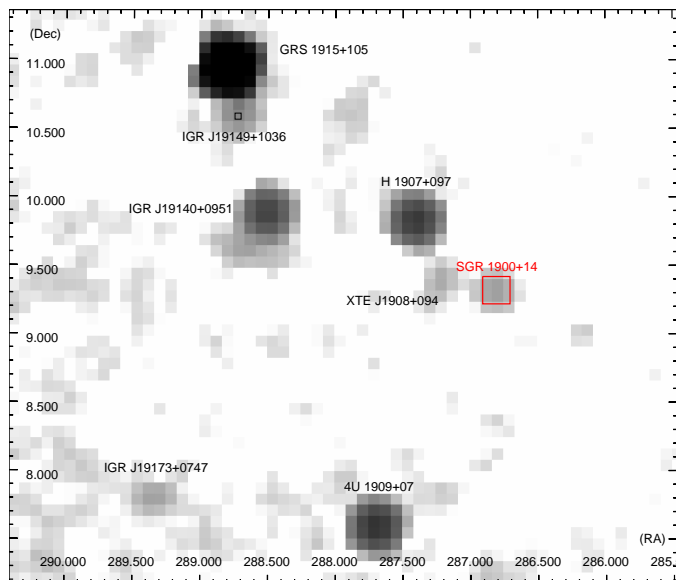


**Fig. 1.** IBIS/ISGRI mosaic image (in  $\text{cts s}^{-1}$ ) of the SGR 1900+14 field in the 22 – 50 keV band.

Ubertini et al. 2003). ISGRI operates in the  $\sim 15$ –400 keV band. IBIS has a fully coded field of view of  $9^\circ \times 9^\circ$  and a partially coded field of view of  $29^\circ \times 29^\circ$ .

We performed the reduction and analysis of IBIS/ISGRI data using the Off-line Science Analysis (OSA) 10.1 software provided by the ISDC Data Centre for Astrophysics (Goldwurm et al. 2003; Courvoisier et al. 2003). We analysed all the public data between 2003 March and 2013 June where SGR 1900+14 was within  $12^\circ$  from the centre of the IBIS/ISGRI field of view. At larger off-axis angle the IBIS response is not well known<sup>1</sup>. We excluded all the data taken during bad time intervals. The resulting data set consists of 4706 pointings, corresponding to an exposure time of  $\sim 11.6$  Ms.

Sky images of each pointing were generated in the energy band 22 – 50 keV. SGR 1900+14 was never detected, being below the  $5\sigma$  threshold of detection, in the individual images.

We combined the individual images of the whole data set to produce the total (mosaic) image (see Fig. 1), in which SGR 1900+14 is detected with a significance of  $9.3\sigma$ . The pixel significance distribution of a sky image obtained from the convolution of the detector image<sup>2</sup> with a decoding array is expected to be Gaussian with zero mean and unitary standard deviation. Systematic errors that are not taken into account by the algorithm that reconstructs the sky image can lead to a broadening of this distribution (Fenimore & Cannon 1978). Systematic effects in the reconstructed image can be originated by the imperfect knowledge of the real instrument and can particularly affect observations of crowded regions of the Galaxy (e.g. Krivonos et al. 2010). We fitted the pixel significance distribution with a Gaussian with standard deviation of 1.18. Therefore, the significance of detection is reduced to  $9.3\sigma/1.18 \approx 7.9\sigma$  (for further details, see e.g. Bélanger et al. 2006; Li et al. 2011).

<sup>1</sup> See the INTEGRAL data analysis documentation: <http://www.isdc.unige.ch/integral/analysis>

<sup>2</sup> The detector image is the shadowgram projected by the coded mask of the telescope on the detector plane.

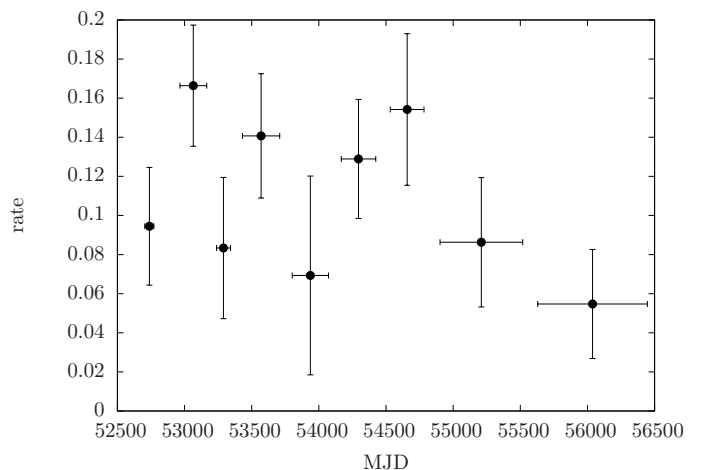


**Fig. 2.** 22 – 50 keV IBIS/ISGRI lightcurve of SGR 1900+14. Time intervals and rates are reported in Table 1.

**Table 1.** Time intervals and intensities (22 – 50 keV) of the nine bins of the lightcurve of SGR 1900+14 (Fig. 2). Errors are at  $1\sigma$  confidence level.

Obs. Number	$T_{\text{start}}$ (MJD)	$T_{\text{stop}}$ (MJD)	$\text{cts s}^{-1}$
1	52704.14	52772.10	$0.09 \pm 0.03$
2	52965.66	53164.83	$0.17 \pm 0.03$
3	53237.98	53341.66	$0.08 \pm 0.04$
4	53431.43	53708.42	$0.14 \pm 0.03$
5	53801.93	54072.02	$0.07 \pm 0.05$
6	54166.75	54424.11	$0.13 \pm 0.03$
7	54531.73	54783.05	$0.15 \pm 0.04$
8	54902.04	55518.02	$0.09 \pm 0.03$
9	55629.45	56446.46	$0.06 \pm 0.03$

## 2.1. Lightcurve analysis

We produced a lightcurve of SGR 1900+14 (Fig. 2) extracting the fluxes from nine mosaic images corresponding to the time intervals indicated in Table 1. Fitting these points with a constant, we obtain a reduced  $\chi^2 = 1.48$  (8 d.o.f.). Since this value has a large probability ( $\sim 16\%$ ) of being obtained by a constant source, we conclude that there is no evidence for variability in the INTEGRAL data. Note, however, that the large error bars of the measured hard X-ray count rates do not allow us to reveal relatively small flux variations, such as those measured for SGR 1900+14 at lower energy. In fact, variations of  $\sim 26\%$  in the soft X-ray flux (0.8–6.5 keV) were detected with *XMM-Newton* and *Chandra* during the period  $\sim 52700$  – 54520 MJD that overlaps that of the INTEGRAL observations analysed in this work (Göğüş et al. 2011). Following Primini et al. (1993), we estimate that our observations could reveal at a  $3\sigma$  confidence level only flux variation larger than  $\sim 130\%$ .

## 2.2. Spectral analysis

We extracted the average spectrum of SGR 1900+14 using the source count rates obtained from the mosaic images in five en-

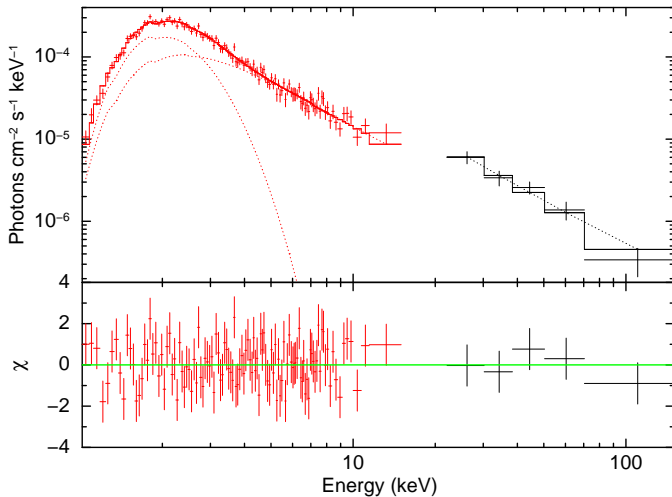


**Fig. 3.** Joint *XMM-Newton* (red), IBIS/ISGRI (black) spectrum fitted with an absorbed power law plus a blackbody model, with residuals in units of standard deviations.

energy bands (22–30, 30–38, 38–50, 50–70, 70–150 keV) using the OSA tool `mosaic_spec`, which is particularly suited for faint sources. We used the exposure-weighted average ancillary response file and the rebinned response matrix specifically generated for our particular data set. Before fitting, we added systematic uncertainties of 5% to the data set. We obtained a good fit ( $\chi^2_{\nu} = 0.5$ , 3 d.o.f.) with a power-law ( $\Gamma = 1.9 \pm 0.3$ ; uncertainties are at 90% c.l.) and 20 – 100 keV flux  $F_x = (1.11 \pm 0.17) \times 10^{-11}$  erg cm $^{-2}$  s $^{-1}$ .

Figure 3 shows the joint *XMM-Newton*, IBIS/ISGRI spectrum. We used the IBIS/ISGRI average spectrum obtained from the whole data set and the *XMM-Newton* data obtained on 2005 September 20 when the source was in quiescent state (Mereghetti et al. 2006). The analysis of EPIC-pn data was performed with the *XMM-Newton* Science analysis system (SAS) software, version 14.0.0. We rejected time intervals affected by high background, obtaining a total good exposure time of  $\approx 20$  ks. We included constant factors in the spectral fitting to allow for normalization uncertainties between the instruments and differences between the soft and hard X-ray spectra due to source variability and not simultaneous observations. We obtained acceptable fit ( $\chi^2_{\nu} = 1.051$ ; 116 d.o.f.) of the joint *XMM-Newton*, IBIS/ISGRI spectrum with an absorbed ( $N_{\text{H}} = 2.5 \pm 0.2 \times 10^{22}$  cm $^{-2}$ ) blackbody ( $kT = 0.41 \pm 0.04$  keV) plus a power-law component ( $\Gamma = 1.87 \pm 0.17$ ). These parameters are consistent with those derived by Mereghetti et al. (2006) from the *XMM-Newton* data alone.

### 3. Discussion

We analysed 11.6 Ms of INTEGRAL data of SGR 1900+14, obtained from 2003 March to 2013 June. We found that the 22 – 150 keV spectrum is well fit by a power law with  $\Gamma = 1.9 \pm 0.3$  and flux  $(1.11 \pm 0.17) \times 10^{-11}$  erg cm $^{-2}$  s $^{-1}$ . A good agreement is found between the IBIS/ISGRI power law photon-index and the soft one, measured below  $\sim 10$  keV with *XMM-Newton* during a quiescent state in 2005 (Mereghetti et al. 2006). The photon-index and significance of SGR 1900+14 presented here are significantly different from those obtained by Götz et al. (2006) ( $\Gamma = 3.1 \pm 0.5$ , significance of  $9\sigma$ ) which were based on

INTEGRAL data collected in the period 2003 March – 2004 June (corresponding to Obs. number 1 of Table 1) and analysed with OSA 5.1. A comparison between the images obtained with OSA 10.1 and OSA 5.1 suggests that the discrepancy in the results might be caused by the substantial improvement of the software that reconstructs the images of the sky from the shadowgram projected by the coded mask onto the detector plane. The images processed with OSA 5.1 showed spurious features, due to residual un-subtracted coding noise, caused by the brightest source in the field of view, GRS 1915+105, which contaminated the spectrum of SGR 1900+14. Such features are not present anymore in the images reconstructed with OSA 10.1. Therefore, the spectral results reported here supersede those of Götz et al. (2006).

The slope of the hard X-ray spectrum derived with INTEGRAL is consistent with that measured with *BeppoSAX* before the giant flare of 1998, but the 20 – 100 keV luminosity ( $\approx 3 \times 10^{35}$  erg s $^{-1}$  for  $d = 15$  kpc, Vrba et al. 2000) is smaller by a factor  $\sim 5$ . A similar decrease of the flux has been observed in the soft band, below  $\sim 10$  keV (Mereghetti et al. 2006; Göğüş et al. 2011).

Kaspi & Boydston (2010) noted an anti-correlation of the spectral turnover  $\Gamma_s - \Gamma_h$  (where  $\Gamma_s$  is the photon-index in the soft band,  $\lesssim 10$  keV, and  $\Gamma_h$  is the photon-index in the hard band,  $\gtrsim 10$  keV) with inferred magnetic field  $B$  and spin-down  $\dot{\nu}$ . These authors gave a qualitative interpretation for the anti-correlation  $\Gamma_s - \Gamma_h$  vs  $B$  in the framework of models in which the X-ray emission of magnetars strongly depends on magnetospheric currents. For magnetars with higher  $B$ ,  $\Gamma_s$  is harder because the scattering optical depth between the relativistic electrons and the surface thermal photons increases. This in turn has an effect on the population of electrons that do not scatter and instead impact on the surface, heating it and creating a corona: fewer electrons will impact on the surface, resulting in a softer  $\Gamma_h$ .

Figure 4 shows an updated version of the plots  $\Gamma_s - \Gamma_h$  vs  $B$  and  $\dot{\nu}$ . Besides the magnetars considered by Kaspi & Boydston (2010) and Vogel et al. (2014) (1E 2259+568, 4U 0142+61, 1RXS 1708–40, SGR 1900+14, 1E 1841–045, and SGR 1806–20), we included our new result for SGR 1900+14 and the pulsed flux of 1E 2259+568 from Vogel et al. (2014). To quantify the significance of the anticorrelation, we determined the Pearson’s linear coefficient  $r$  and the null hypothesis probability  $p$ . For the total flux data, we found  $r = -0.97$ ,  $p = 0.0012$  and  $r = -0.96$ ,  $p = 0.0025$ , for  $\Gamma_s - \Gamma_h$  as function of  $B$  and  $\dot{\nu}$ , respectively. For the pulsed data, we found  $r = -0.98$ ,  $p = 0.0157$  and  $r = -0.98$ ,  $p = 0.0236$  for  $\Gamma_s - \Gamma_h$  as function of  $B$  and  $\dot{\nu}$ , respectively. The new value of the spectral turnovers of SGR 1900+14 ( $0.06 \pm 0.23$  compared to the previous value  $-1.2 \pm 0.5$ ) and 1E 2259+568 (Vogel et al. 2014) improve the significance of the anticorrelation measured by Kaspi & Boydston (2010). We used a linear model to fit the data ( $\Gamma_s - \Gamma_h = a + b \log_{10} x$ , where  $x = B$  or  $x = \dot{\nu}$ ). For  $\Gamma_s - \Gamma_h$  as function of  $B$  and total flux data set we found  $a = 46 \pm 2$ ,  $b = -3.04 \pm 0.14$ ,  $\chi^2 = 15.9$  (4 d.o.f.). For the pulsed flux we obtained  $a = 53 \pm 3$ ,  $b = -3.5 \pm 0.2$ ,  $\chi^2 = 9.2$  (2 d.o.f.). When considering  $\Gamma_s - \Gamma_h$  as function of  $\dot{\nu}$ , we found for total flux:  $a = -17.4 \pm 0.9$ ,  $b = -1.51 \pm 0.07$ ,  $\chi^2 = 29.9$  (4 d.o.f.); for the pulsed flux:  $a = -29 \pm 3$ ,  $b = -2.4 \pm 0.2$ ,  $\chi^2 = 8.3$ , (2 d.o.f.). A quadratic model ( $\Gamma_s - \Gamma_h = a + b \log_{10} \dot{\nu} + c(\log_{10} \dot{\nu})^2$ ) fits better the total flux data:  $a = 65 \pm 15$ ,  $b = 12 \pm 2$ ,  $c = 0.5 \pm 0.1$ ,  $\chi^2 = 2.1$  (3 d.o.f.). Best fit models are shown in Figure 4.

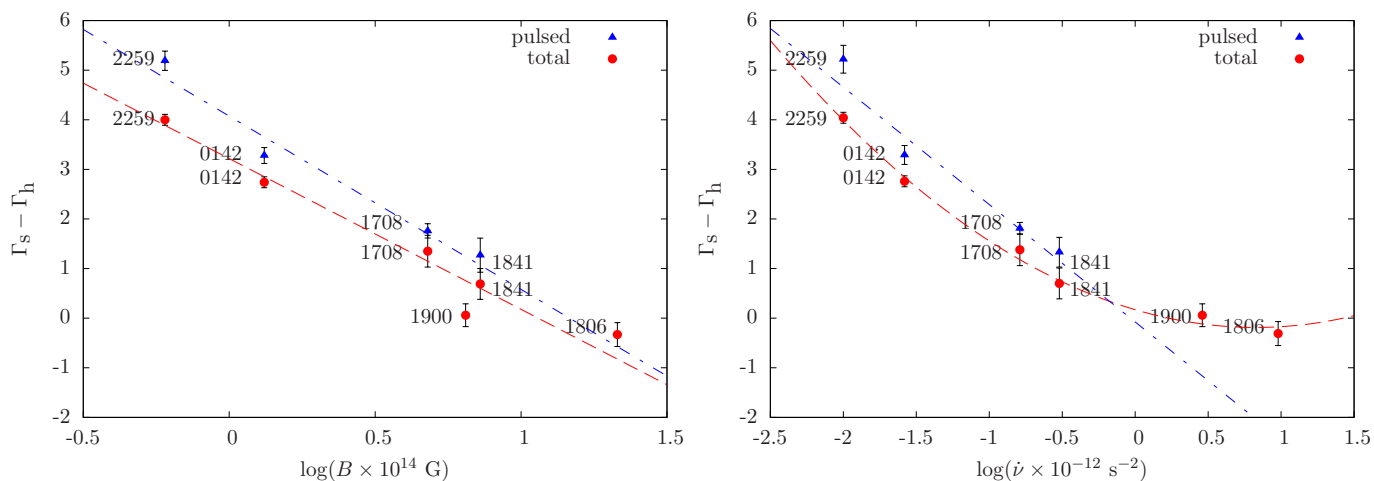


**Fig. 4.** Spectral turnover  $\Gamma_s - \Gamma_h$  as function of the magnetic field  $B$  (left panel) and spin-down  $\dot{\nu}$  (right panel) for all magnetars for which  $\Gamma_s$  and  $\Gamma_h$  are measured. Red circles represent total flux and blue triangles represent pulsed flux. Error bars represent  $1\sigma$  uncertainties. Linear fits are shown on the left panel, both for pulsed flux (blue line) and total flux (red line), and on the right panel for pulsed flux (blue line). For total flux data in the right panel, the best-fitting quadratic trend is shown. The figure is an updated version of figure 9 of Vogel et al. (2014), with the new value of  $\Gamma_s - \Gamma_h$  for SGR 1900+14 obtained in this work.

## 4. Conclusions

We have reported a new analysis of the hard X-ray emission from SGR 1900+14 based on ten years of observations with the IBIS/ISGRI instrument on the INTEGRAL satellite. Due to the improved calibrations and analysis software, we obtained results which differ from and supersede those reported earlier for this source and based only on the first two years of data. We measured a 20–100 keV flux of  $F_x = (1.11 \pm 0.17) \times 10^{-11}$  erg cm $^{-2}$  s $^{-1}$ , which is lower than that seen in 1997 with *BeppoSAX* by a factor of  $\sim 5$ . While the previously found photon index at  $E > 20$  keV indicated a power law spectrum significantly softer than those of other SGRs and AXPs, the new value of  $1.9 \pm 0.3$  is similar to those found for the other sources and to that measured at lower energy for SGR 1900+14.

*Acknowledgements.* This work is partially supported by the Bundesministerium für Wirtschaft und Technologie through the Deutsches Zentrum für Luft und Raumfahrt (grant FKZ 50 OG 1301). This work has been partially supported through financial contribution from the agreement ASI/INAF I/037/12/0 and from PRIN INAF 2014. This paper is based on data from observations with INTEGRAL, and *XMM-Newton*. INTEGRAL is an ESA project with instruments and science data centre funded by ESA member states (especially the PI countries: Denmark, France, Germany, Italy, Spain, and Switzerland), Czech Republic and Poland, and with the participation of Russia and the USA. *XMM-Newton* is an ESA science mission with instruments and contributions directly funded by ESA Member States and NASA. This research has made use of data and/or software provided by the High Energy Astrophysics Science Archive Research Center (HEASARC), which is a service of the Astrophysics Science Division at NASA/GSFC and the High Energy Astrophysics Division of the Smithsonian Astrophysical Observatory. This research has made use of SAOImage DS9, developed by Smithsonian Astrophysical Observatory.

## References

- Bélangier, G., Goldwurm, A., Renaud, M., et al. 2006, ApJ, 636, 275  
 Courvoisier, T. J.-L., Walter, R., Beckmann, V., et al. 2003, A&A, 411, L53  
 Esposito, P., Mereghetti, S., Tiengo, A., et al. 2007, A&A, 461, 605  
 Fenimore, E. E. & Cannon, T. M. 1978, Appl. Opt., 17, 337  
 Frontera, F., Costa, E., dal Fiume, D., et al. 1997, A&AS, 122, 357  
 Goldwurm, A., David, P., Foschini, L., et al. 2003, A&A, 411, L223  
 Golenetskii, S., Aptekar, R., Mazets, E., et al. 2006, GRB Coordinates Network, 4936, 1  
 Götz, D., Mereghetti, S., Tiengo, A., & Esposito, P. 2006, A&A, 449, L31

- Gögüş, E., Güver, T., Özel, F., Eichler, D., & Kouveliotou, C. 2011, ApJ, 728, 160  
 Hurley, K., Mazets, E., Golenetskii, S., & Cline, T. 2002, GRB Coordinates Network, 1715, 1  
 Kaspi, V. M. & Boydston, K. 2010, ApJ, 710, L115  
 Krivonos, R., Revnivtsev, M., Tsygankov, S., et al. 2010, A&A, 519, A107  
 Lebrun, F., Leray, J. P., Lavocat, P., et al. 2003, A&A, 411, L141  
 Li, J., Torres, D. F., Chen, Y., et al. 2011, ApJ, 738, L31  
 Mereghetti, S., Esposito, P., Tiengo, A., et al. 2006, ApJ, 653, 1423  
 Mereghetti, S., Pons, J. A., & Melatos, A. 2015, Space Sci. Rev.[arXiv:1503.06313]  
 Nakagawa, Y. E., Mihara, T., Yoshida, A., et al. 2009, PASJ, 61, 387  
 Primini, F. A., Forman, W., & Jones, C. 1993, ApJ, 410, 615  
 Tiengo, A., Esposito, P., Mereghetti, S., et al. 2007, Ap&SS, 308, 33  
 Ubertini, P., Lebrun, F., Di Cocco, G., et al. 2003, A&A, 411, L131  
 Vetere, L., Barthelmy, S. D., Kennea, J. A., Markwardt, C. B., & Palmer, D. M. 2006, GRB Coordinates Network, 4922, 1  
 Vogel, J. K., Hascoët, R., Kaspi, V. M., et al. 2014, ApJ, 789, 75  
 Vrba, F. J., Henden, A. A., Luginbuhl, C. B., et al. 2000, ApJ, 533, L17  
 Winkler, C., Courvoisier, T. J.-L., Di Cocco, G., et al. 2003, A&A, 411, L1